Journal of Molecular Graphics and Modelling 27 (2008) 197–208

Contents lists available at ScienceDirect

Journal of Molecular Graphics and Modelling

journal homepage: www.elsevier.com/locate/JMGM

# An investigation of structurally diverse carbamates for acetylcholinesterase (AChE) inhibition using 3D-QSAR analysis

Kuldeep K. Roy, Anshuman Dixit, Anil K. Saxena [1,*]

*Medicinal and Process Chemistry Division, Central Drug Research Institute, Lucknow 226001, U.P., India*

ARTICLE INFO

*Article history:*
Received 11 February 2008
Received in revised form 10 April 2008
Accepted 14 April 2008
Available online 24 April 2008

*Keywords:*
Acetylcholinesterase
Carbamates
QSAR
CoMFA
CoMSIA
Pharmacophore

ABSTRACT

In order to identify the essential structural features and physicochemical properties for acetylcholinesterase (AChE) inhibitory activity in some carbamate derivatives, the systematic QSAR (Quantitative Structure Activity Relationship) studies (CoMFA, advance CoMFA and CoMSIA) have been carried out on a series of (total 78 molecules) taking 52 and 26 molecules in training and test set, respectively.

Statistically significant 3D-QSAR (three-dimensional Quantitative Structure Activity Relationship) models were developed on training set molecules using CoMFA and CoMSIA and validated against test set compounds. The highly predictive models (CoMFA $q^2 = 0.733$, $r^2 = 0.967$, predictive $r^2 = 0.732$, CoMSIA $q^2 = 0.641$, $r^2 = 0.936$, predictive $r^2 = 0.812$) well explained the variance in binding affinities both for the training and the test set compounds. The generated models suggest that steric, electrostatic and hydrophobic interactions play an important role in describing the variation in binding affinity. In particular the carbamoyl nitrogen should be more electropositive; substitutions on this nitrogen should have high steric bulk and hydrophobicity while the amino nitrogen should be electronegative in order to have better activity. These studies may provide important insights into structural variations leading to the development of novel AChE inhibitors which may be useful in the development of novel molecules for the treatment of Alzheimer's disease.



## 1. Introduction

The Alzheimer's disease (AD) is characterized by a progressive impairment in memory and intellectual ability, accompanied by behavioral disturbances and the person affected may not recognize family members or may have trouble speaking, reading or writing and in carrying out daily activities [1]. The enzyme, acetylcholinesterase (AChE), is responsible for the termination of impulse signaling at cholinergic synapses by catalyzing the hydrolysis of the neurotransmitter acetylcholine (ACh) and is also a promising drug-like target for the treatment of Alzheimer's disease [2]. In fact it is one of the targets viz. AChE and *N*-methyl-D-aspartate (NMDA) that has provided few palliative drugs presently marketed for the treatment of Alzheimer's disease. These drugs include tacrine, galanthamine, donepezil, and rivastigmine as acetylcholinesterase inhibitors (AChEI) and memantine as a non-competitive NMDA antagonist for moderate improvement in memory and cognitive function [3–9]. The active site of AChE consists of an esteratic subsite containing the catalytic functional unit, and an anionic subsite responsible for binding the quaternary trimethylammonium tail group of ACh. The catalytic functional unit of AChE is the catalytic triad consisting of *Ser200*, *Glu327*, and *His440*. The structure of the gorge also reveals a constricted region formed by the side chains of *Tyr124*, *Phe297*, *Tyr337*, and *Phe338*. An allosteric site located at the periphery of the gorge also plays an important role in ligand binding. This site called the peripheral anionic site (PAS) is composed of surface residues *Tyr70*, *Asp72*, *Tyr121*, *Tyr334* and *Trp279* [10,11].

A lot of research has been directed towards modulating the AChE inhibitory activity by using different substitutions in carbamate series and a number of useful leads have been generated, e.g. Weinstock et al. have reported a relationship between chemical structure and AChE inhibitory activity in a series of mono- and dialkyl 3-(1-dimethylamino ethyl)-phenyl carbamates [12,13]. The authors showed a close correlation between the amount of energy needed to overcome the restriction of rotation about the amide bond (Delta Gq) and the affinity of the inhibitor ($K_i$) for the AChE enzyme. The anomalous "ethyl" effect was observed by Lieske et al. [14] who found that the diethyl carbamoyl derivative is the least active in a series of 5-(1,3,3-trimethylindolinyl) carbamates, about 7400 times less potent ($K_i$) than the dimethylcarbamoyl analogues. Among monosubstituted carbamates, the compounds substituted by a propyl group were

* Corresponding author. Tel.: +91 522 2612412x4386; fax: +91 522 26123405.
*E-mail address:* anilsak@gmail.com (A.K. Saxena).
[1] CDRI Communication No. 7499.

1093-3263/$ – see front matter © 2008 Elsevier Inc. All rights reserved.
doi:10.1016/j.jmgm.2008.04.006

**Table 1**
AChE inhibitory activities ($IC_{50}$, μM) of 1-aminoindane, 1- or 2-aminotetraline, and phenethylamine carbamates

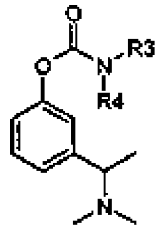


1-2

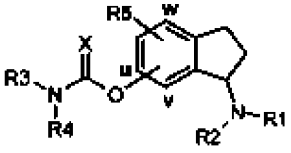


3-19, 24-48, 53-55

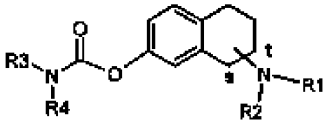


20-23, 49-52

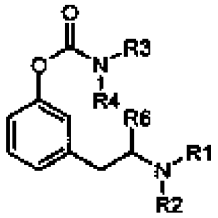


56-78

| Comp. | $R_1$ | $R_2$ | $R_3$ | $R_4$ | $R_5$ | $R_6$ | O | *N* | $IC_{50}$ | $pIC_{50}$ |
|---|---|---|---|---|---|---|---|---|---|---|
| 1 | – | – | Me | Me | H | – | – | | 0.03 | 1.52 |
| 2[a] | – | – | Me | Et | H | – | – | | 0.92 | 0.04 |
| 3[a] | H | H | Me | Me | H | – | u | | 0.76 | 0.12 |
| 4 | H | H | Me | Et | H | – | u | | 19.00 | −1.28 |
| 5[a] | H | H | Me | *n*-Pro | H | – | u | | 7.30 | −0.86 |
| 6 | H | H | Me | *n*-hexyl | H | – | u | | 0.53 | 0.28 |
| 7[a] | H | H | Me | cyclohexyl | H | – | u | | 3.96 | −0.60 |
| 8 | H | H | Me | *p*-MeOPh | H | – | u | | 0.30 | 0.52 |
| 9[a] | H | H | H | Et | H | – | u | | 17.70 | −1.25 |
| 10 | H | H | H | *n*-Pro | H | – | u | | 1.48 | −1.70 |
| 11[a] | H | Me | Me | Me | H | – | u | | 1.07 | −0.03 |
| 12 | H | Me | Me | Et | H | – | u | | 38.60 | −1.59 |
| 13[a] | H | Et | Me | Me | H | – | u | | 24.50 | −1.39 |
| 14[a] | H | *n*-Pro | Me | Et | H | – | u | | 3.60 | −0.56 |
| 15 | H | H | Me | Me | H | – | v | | 0.46 | 0.34 |
| 16[a] | H | H | Me | Et | H | – | v | | 10.50 | −1.02 |
| 17[a] | H | H | Me | Me | H | – | v | | 0.51 | 0.29 |
| 18 | H | H | Me | Me | H | – | w | | 0.009 | 2.05 |
| 19[a] | H | H | Me | Et | H | – | w | | 0.026 | 1.59 |
| 20 | H | H | Me | Me | H | – | u | s | 1.48 | −0.17 |
| 21[a] | H | H | Me | Et | H | – | u | s | 6.22 | −0.79 |
| 22 | H | H | Me | Me | H | – | u | t | 3.24 | −0.51 |
| 23[a] | H | H | Me | Et | H | – | u | t | 79.60 | −1.90 |
| 24 | H | Pg | Me | Me | H | – | u | | 2.90 | −0.46 |
| 25[a] | H | Pg | Me | Et | H | – | u | | 47.00 | −1.67 |
| 26 | H | Pg | Me | *n*-Pro | H | – | u | | 14.60 | −1.16 |
| 27 | H | Pg | Me | *n*-hexyl | H | – | u | | 15.70 | −1.20 |
| 28 | H | Pg | Me | cyclohexyl | H | – | u | | 41.20 | −1.62 |
| 29[a] | H | Pg | Me | *p*-MeOPh | H | – | u | | 0.86 | 0.07 |
| 30 | H | Pg | H | Et | H | – | u | | 13.70 | −1.14 |
| 31 | H | Pg | H | *n*-Pro | H | – | u | | 2.38 | −0.38 |
| 32 | H | Pg | Me | *n*-Bu | H | – | u | | 11.30 | −1.05 |
| 33[a] | H | Pg | Et | *n*-Bu | H | – | u | | 72.40 | −1.86 |
| 34 | H | Pg | Me | cyclohexyl | H | – | u | | 17.90 | −1.25 |
| 35 | H | Pg | Me | Bn | H | – | u | | 1.78 | −0.25 |
| 36[a] | H | Pg | Me | Ph | H | – | u | | 0.55 | 0.26 |
| 37 | Me | Pg | Me | Me | H | – | u | | 12.90 | −1.11 |
| 38 | Et | Pg | Me | Me | H | – | u | | 17.90 | −1.25 |
| 39 | H | Pg | Me | Me | H | – | v | | 2.50 | −0.40 |
| 40 | H | Pg | Me | Et | H | – | v | | 525.00 | −2.72 |
| 41 | H | Pg | Me | *n*-Pro | H | – | v | | 45.80 | −1.66 |
| 42 | Me | Pg | Me | Me | H | – | v | | 7.00 | −0.85 |
| 43[a] | Me | Pg | Me | Et | H | – | v | | 439.00 | −2.64 |
| 44[a] | H | Pg | Me | Me | H | – | w | | 0.053 | 1.28 |
| 45 | H | Pg | Me | Et | H | – | w | | 2.15 | −0.33 |
| 46 | H | Pg | Me | Et | 5-Cl | – | u | | 25.50 | −1.41 |
| 47 | H | Pg | Me | *n*-Pr | 5-Cl | – | u | | 43.90 | −1.64 |
| 48 | H | 1-MePg | Me | Me | H | – | u | | 1.80 | −0.25 |
| 49 | H | Pg | Me | Me | H | – | u | s | 3.94 | −0.60 |
| 50[a] | H | Pg | Me | Et | H | – | u | s | 52.40 | −1.72 |
| 51 | H | Pg | Me | Me | H | – | u | t | 4.10 | −0.61 |
| 52 | H | Pg | Me | Et | H | – | u | t | 204.00 | −2.31 |
| 53 | Me | Pg | Me | Et | H | – | w | | 14.90 | −1.17 |
| 54 | Me | Me | Me | Me | H | – | u | | 2.15 | −0.33 |
| 55[a] | Me | Me | Me | Me | H | – | w | | 0.013 | 1.89 |
| 56 | H | H | Me | Me | H | H | – | | 0.23 | 0.64 |
| 57 | H | H | Me | Et | H | H | – | | 35.50 | −1.56 |
| 58 | H | H | Me | *n*-Pro | H | H | – | | 7.80 | −0.89 |
| 59 | H | Me | Me | Me | H | H | – | | 0.28 | 0.55 |
| 60[a] | H | Me | Me | Et | H | H | – | | 20.70 | −1.32 |
| 61 | Me | Me | Me | Me | H | H | – | | 0.16 | 0.76 |

**Table 1** (*Continued*)

| Comp. | $R_1$ | $R_2$ | $R_3$ | $R_4$ | $R_5$ | $R_6$ | O | *N* | $IC_{50}$ | $pIC_{50}$ |
|---|---|---|---|---|---|---|---|---|---|---|
| 62 | H | Pg | Me | Me | H | H | – | | 0.22 | 0.66 |
| 63 | H | Pg | Me | Et | H | H | – | | 30.20 | −1.48 |
| 64 | H | Pg | Me | *n*-Pro | H | H | – | | 15.40 | −1.19 |
| 65[a] | Me | Pg | Me | Me | H | H | – | | 0.85 | 0.07 |
| 66 | Me | Pg | Me | Et | H | H | – | | 16.60 | −1.22 |
| 67 | H | Pg | Me | Me | H | Me | – | | 0.54 | 0.27 |
| 68 | H | Pg | Me | Et | H | Me | – | | 33.90 | −1.53 |
| 69 | H | Pg | Me | *n*-Pro | H | Me | – | | 19.10 | −1.28 |
| 70[a] | H | Pg | Me | cyclohexyl | H | Me | – | | 3.60 | 0.56 |
| 71 | H | Pg | Me | *n*-Bu | H | Me | – | | 12.20 | −1.09 |
| 72[a] | Me | Pg | Me | Me | H | Me | – | | 1.64 | −0.22 |
| 73 | Me | Pg | Me | Et | H | Me | – | | 234.00 | −2.37 |
| 74 | Me | Pg | Me | *n*-Pro | H | Me | – | | 33.10 | −1.52 |
| 75 | Me | Pg | Me | *n*-hexyl | H | Me | – | | 3.06 | −0.49 |
| 76 | Me | Pg | Me | cyclohexyl | H | Me | – | | 8.67 | −0.94 |
| 77[a] | H | 1-MePg | Me | Me | H | Me | – | | 0.17 | 0.77 |
| 78 | H | 1-MePg | Me | Et | H | Me | – | | 13.90 | −1.14 |

[a] The compounds taken in the test set; Pg = propargyl; *n*-Pro = *N*-propyl; *c*-Hexyl = cyclohexyl; 1-MePg = 1-methyl-2-propynyl; Bn = benzyl; Me = methyl; Et = ethyl; *n*-Bu = *n*-butyl; *p*-MeOPh = *p*-methoxyphenyl; Ph = phenyl.

suggested to be more active than their corresponding ethyl analogs similar to the carbamates reported by Weinstock et al. [12,13].

The ligand based approaches like three-dimensional Quantitative Structure Activity Relationship (3D-QSAR) studies have been quite useful in identifying the essential structural requirements for enzyme inhibitory activity. Though some 2D-QSAR studies have been reported on Biphenyl-4-acyoxylate-4′-*N*-butylcarbamates [15,16] in order to probe the peripheral anionic site, composed of *Trp279*, *Tyr70*, *Tyr121*, and *Asp72*, in the AChE and butyrylcholinesterase (BChE) for pseudo-reversible inhibition but neither 2D- nor 3D-QSAR studies have been carried out to probe the esteratic subsite containing the catalytic functional unit comprising of *Ser 200*, *Glu 327*, and *His 440*, and an anionic subsite composed of *Trp84*, *Glu199*, and *Phe330* responsible for binding the quaternary trimethylammonium tail group of ACh. Therefore, it appeared of interest to carry out Comparative Molecular Field Analysis or CoMFA and Comparative Molecular Similarity Indices Analysis or CoMSIA studies on the carbamates for their AChE inhibitory activity. These studies are reported in this paper.

## 2. Materials and methods

### 2.1. Biological data

The 3D-QSAR studies were performed on 78 chemically diverse molecules belonging to substituted carbamoyl aminoindanes, tetralenes and phenethyl amines (Table 1) reported by Sterling et al. [17]. The AChE inhibitory activity of the compounds is expressed as $IC_{50}$ value in the micromolar (μM) range. The selected compounds cover a wide range of biological activity spanning over five log units (0.009–525 μM) and diverse structural features. The $IC_{50}$ values were converted into log $IC_{50}$ ($pIC_{50}$) for use in the QSAR studies.

### 2.2. Rational division of training and test sets

In view of the recent finding that $q^2$ appears to be the necessary but not the sufficient condition for the model to have a high predictive power [18a,b], the emphasis has been given for the validation on an external test set. It has been suggested that the models should be tested on a sufficiently large test set (25–33% of total) to establish a reliable QSAR model [18b]. Among several methods for the classification of the dataset into training and test sets viz. random sampling (RS), activity ranked clustering (ARC) and descriptor based clustering (DBC); the DBC has been shown to be the most effective method for selection of representative test set (both in terms of activity and structural diversity). Therefore, the compounds were rationally divided into training (52 compounds) and test (26 compounds) sets by CoMFA based hierarchical clustering using molecular steric and electrostatic fields as parameters. The test set compounds were picked up from generated clusters (13) in such a way that they cover almost entire range of biological activity. Thus both the sets (training and test) span full range of biological activity and structural features and the test set can be reasonably used to validate the generated QSAR models.

### 2.3. Computational details

The molecular modeling studies CoMFA, advanced CoMFA and CoMSIA were performed on a Silicon Graphics Octane R12000 workstation using SYBYL 6.9 molecular modeling software [19]. The structures were built from fragments in SYBYL fragment library. The partial charges were calculated using Gasteiger–Hückel method and their geometry was optimized using Tripos force field with a distance-dependent dielectric function until a root mean square (rms) deviation of 0.01 kcal/mol Å was achieved. The conformational search was performed using multisearch method with the following settings: maximum cycles (400), maximum conformers (400), energy cutoff (70 kcal/mol), maximum rms gradient (3.0) tolerance (0.40), and number of hit (12). The minimum energy conformations thus obtained were used in the analysis.

### 2.4. Molecular alignments

Structural alignment is perhaps the most subjective, yet critical, step in CoMFA study. The experience shows that the resulting 3D-QSAR models are often sensitive to a particular alignment scheme. However in contrast to CoMFA, CoMSIA is relatively less sensitive to changes in orientation of the superimposed molecules in the lattice [20]. Therefore, in the present study we compared three different alignment rules carefully to get the most efficient one for such structurally diverse molecules.

1. *The common substructure fitting method* (Alignment 1). In this method, molecules are superimposed to a common substructure (Fig. 1A).
2. *The flexible fitting (multi-fit) method* (Alignment 2). The alignment of molecules is performed by a multi-fit option, allowing

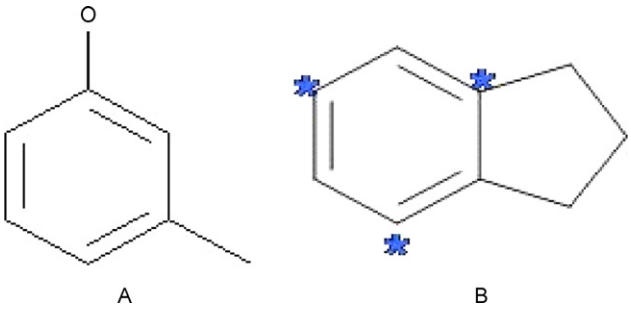


**Fig. 1.** (A) Substructure for common substructure based alignment and (B) substructure with asterisk marks indicating atoms used for multi-fit alignment.

flexible fitting of the molecules to the template. The atoms (asterisk marked in Fig. 1B) were considered as fitting point.

3. *The rigid body field-fit method* (Alignment 3). In this procedure, the root mean square differences (RMSD) between the molecules and the template molecule for steric and electrostatic fields, averaged across all lattice points, is minimized.

In 'Common substructure fitting method', the 3D structures of the molecules to be analyzed are aligned to a suitable conformational template, which is assumed to adopt a "bioactive conformation". The compounds were fitted to the template molecule **18** which is the most active molecule in the dataset. In order to optimize the alignment different substructures were used and the best alignment was selected from different alignments thus generated. The most successful alignment was achieved by using the common aryloxy substructure (Fig. 1A). This alignment placed less significance on substituted or unsubstituted amino groups and correspondingly more significance on the carbamate groups. Among different alignments this alignment yielded the best results, though it resulted in flipping of the indane ring in 4- and 7-carbamates. It can be seen the position of carbamate groups is same while the indane, tetralene and phenethyl groups are taking different orientations (Fig. 2).

The multi-fit based alignment (Alignment 2) where the attempt was made to place nitrogen (of indane, tetralene and phenethyl groups) together resulted in scattering of carbamate groups and the field-fit alignment (Alignment 3) in which the molecules were somewhat scattered due to their rigid nature and relative position of different groups did not show any significant improvement in terms of statistical parameters including leave one out (LOO) cross-validation, $q^2$ over the first common substructure based alignment (Table 2).

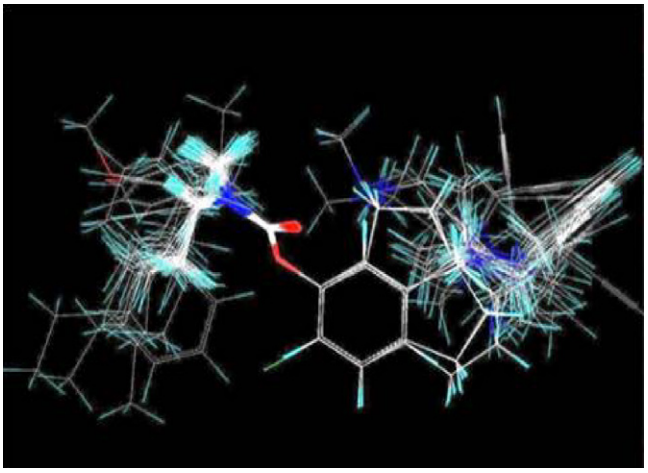

**Fig. 2.** Common substructure based alignment of all 78 molecules.

### 2.5. CoMFA [21] studies

#### 2.5.1. CoMFA

The aligned molecules were kept in a 3D cubic lattice with a grid spacing of 2.0 Å in *x*, *y* and *z* directions. The steric (6–12 Lennard–Jones potential) and electrostatic (Columbic with $1/r$ dielectric) fields were calculated at each lattice point using Tripos force field and distance-dependent dielectric constant. A $sp^3$-hybridized carbon with a +1.0 charge was used as a probe atom. To avoid too high and unrealistic energy values inside the molecule, a 30 kcal/mol energy cutoff was applied.

#### 2.5.2. Advance CoMFA

H-bonding (HB), indicator (IND) and parabolic (PBL) fields are used in advanced CoMFA routine to extend the scope of CoMFA. H-bond fields are special indicator fields based on the description by Bohacek and McMartin [22]. Lattice points with steric energies below the steric cutoff energy are assigned nominal energies equal to the steric cutoff energy if they are close to H-bond accepting or donating atoms. Indicator fields [23] replace all lattice energies with magnitudes below a designated threshold with zero values. All energies at or above that threshold are replaced with a nominal energy value equal in magnitude to the relevant field cutoff value. When both fields are included in a single CoMFA column, the greater of the steric and electrostatic cutoffs is used. The sign of the original lattice energy is retained. Parabolic fields are those in which the magnitude of a standard steric and/or electrostatic field

**Table 2**
The comparative study of three alignments (all 78 molecules)

| Study | Alignment 1 | | Alignment 2 | | Alignment 3 | |
|---|---|---|---|---|---|---|
| | CoMFA | CoMSIA | CoMFA | CoMSIA | CoMFA | CoMSIA |
| Parameters* | TS | SEH | TS | SEH | TS | SEH |
| $q^2$ | 0.730 | 0.755 | 0.637 | 0.476 | 0.152 | 0.046 |
| $s_{press}$ | 0.544 | 0.522 | 0.635 | 0.758 | 0.985 | 1.002 |
| $r^2$ | 0.931 | 0.914 | 0.899 | 0.771 | 0.990 | 0.636 |
| SEE | 0.275 | 0.308 | 0.335 | 0.501 | 0.107 | 0.629 |
| *F* | 159.555 | 106.886 | 88.947 | 39.909 | 746.88 | 43.03 |
| *N* | 6 | 7 | 7 | 6 | 9 | 3 |
| $r^2_{bs}$ | 0.950 | 0.929 | 0.937 | 0.837 | 0.995 | 0.743 |
| $SD_{bs}$ | 0.012 | 0.016 | 0.013 | 0.038 | 0.003 | 0.051 |
| $r^2_{CV(mean)}$ | 0.676 | 0.642 | 0.528 | 0.423 | 0.106 | 0.030 |

$q^2$ = cross-validated correlation coefficient; $s_{press}$ = cross-validated standard error; $r^2$ = determination coefficient; SEE = noncross-validated standard error; *F* = Fischer's *F*-value; *N* = optimal number of components; $r^2_{bs} = r^2$ obtained after bootstrapping; $SD_{bs}$ = bootstrapping standard deviation; $r^2_{CV(mean)}$ = mean $r^2$ of cross-validation in groups; TS = Tripos standard field, *S* = steric, *E* = electrostatic, *H* = hydrophobic field.

at each lattice point has been squared; the original sign of the energy is retained.

### 2.6. CoMSIA [24] studies

CoMSIA is considered superior to CoMFA in certain respects like it is immune to small shifts in regions, remains unaffected when the orientation of molecules is changed; there is no need of strict cutoffs which can result in exclusion of several important data points and more intuitively interpretable contour maps. CoMSIA calculates similarity indices at the intersections of a surrounding lattice. Five similarity fields namely steric, electrostatic, hydrophobic, hydrogen bond donor and acceptor were calculated. The lattice dimensions were selected with a sufficiently large margin extended up to 4 Å surrounding all aligned molecules. In CoMSIA, the steric indices are related to the third power of the atomic radii, the electrostatic descriptors are derived from atomic partial charges, the hydrophobic fields are derived from atom-based parameters, and the hydrogen bond donor and acceptor indices are obtained by a rule-based method derived from experimental values. In the present work, similarity indices were computed using a probe atom with radius 1.0 Å, charge +1, hydrophobicity +1, hydrogen bond donor and acceptor properties of +1 and attenuation factor of 0.3 for the Gaussian type distance function. A Gaussian function is used for the distance dependence between the probe atom and the molecule atoms. Because of the different shape of the Gaussian function, the similarity indices can be calculated at all grid points, both inside and outside the molecular surface.

The equation used to calculate the similarity indices is as follows:

$$A^{q}_{\mathrm{F,k}}(j) = \sum W_{\mathrm{probe,\,k}} W_{ik} \mathrm{e}^{-\alpha r_{2iq}}$$

where $A$ is the similarity index at grid point $q$, summed over all atoms $i$ of the molecule $j$ under investigation. $W_{\mathrm{probe,\,k}}$ is the probe atom with radius 1 Å, charge +1, hydrophobicity +1, hydrogen bond accepting +1, $W_{ik}$, is the actual value of the physicochemical property k of atom $i$, $r_{iq}$ is the mutual distance between the probe atom at grid point $q$ and atom $i$ of the test molecule, $\alpha$ is the attenuation factor, with a default value of 0.3, and an optimal value normally between 0.2 and 0.4.

Larger values result in a steeper Gaussian function, and a strong attenuation of the distance-dependent effects of molecular similarity. Global molecular features become less important, and there is little averaging of local features. With an attenuation factor ($\alpha$) of 0.3, each property value of a given atom is felt by 74.1% at 1 Å from the atom, by 30.1% at 2 Å, and by 6.7% at 3 Å.

### 2.7. Partial least squares (PLS) analysis

PLS was used to correlate the AChE inhibitory activity with the CoMFA and CoMSIA values containing magnitude of steric, electrostatic and other potentials. The generated models were assessed by using LOO cross-validation procedure by SAMPLS method as implied in SYBYL. A strict criterion for selection of optimal number of components was applied by selecting lowest $s_{\mathrm{press}}$ value and also wherever the last added component increased $q^2$ less than 5%, the less complex model was chosen. In addition to LOO cross-validation the cross-validation in groups using ten groups, repeating the procedure 10 times was also carried out. The mean of 10 readings is given as $[r^2_{\mathrm{CV(mean)}}]$. The partial least squares algorithm was used to generate the final CoMFA and CoMSIA models with optimal number of components obtained using LOO cross-validation. The minimum sigma standard deviation threshold was set at 2.0 kcal/mol to speed up the analysis and to reduce the noise. The $r^2_{\mathrm{CV}}$, $s_{\mathrm{press}}$, $r^2$, and SE values were computed as defined in SYBYL.

### 2.8. Predictive $r^2$

The predictive $r^2$ was based only on molecules not considered in the training set. Predictive $r^2$ ($r^2_{\mathrm{pred}}$) value is defined as

$$r^2_{\mathrm{pred}} = \frac{(\mathrm{SD} - \mathrm{PRESS})}{\mathrm{SD}}$$

where SD is the sum of squared deviation between the biological activities of the test set molecule and the mean activity of the training set molecules and PRESS is the sum of squared deviations between the observed and the predicted activities of the test molecules [25]. If $\mathrm{Pr}^2$ is zero, then the results are not by chance and are significant. Like $r^2_{\mathrm{cv}}$, the predictive $r^2$ can assume a negative value reflecting a complete lack of predictive ability of the model of the molecules included in the test set [26]. To further assess the robustness and statistical confidence of the derived models, bootstrapping analysis (100 runs) was performed. CoMFA standard scaling was applied to all the CoMFA analysis while autoscaling was applied to all CoMSIA analysis.

## 3. Results and discussion

The CoMFA and CoMSIA are highly sensitive to the relative alignment of molecules and since these molecules have widely varying structures, it was important to determine the best alignment rule.

The best alignment was selected on the basis of $q^{2-}$ values both for CoMFA and CoMSIA using all 78 compounds. Out of the three alignments, the alignment obtained using the common substructure fitting method (alignment 1) was found to exhibit high $q^2$ values both for CoMFA ($q^2$ = 0.730) as well as CoMSIA ($q^2$ = 0.755). The detailed statistical results obtained for the three alignments taking all molecules are shown in Table 2.

Since the Common Substructure Alignment method gave the model with best statistics and reasonable superimposition of important functional groups (Fig. 2), this alignment was further used for systematic CoMFA, advance CoMFA and CoMSIA studies using the training set compounds (total 52). The results have been summarized in Tables 3 and 4.

**Table 3**
CoMFA and advanced CoMFA models generated using alignment 1

| Parameters | | TS | IND | PBL |
|---|---|---|---|---|
| $q^2$ | | 0.733 | 0.604 | 0.556 |
| $s_{\mathrm{press}}$ | | 0.532 | 0.634 | 0.671 |
| $r^2$ | | 0.967 | 0.939 | 0.915 |
| SEE | | 0.187 | 0.249 | 0.293 |
| $F$ | | 185.412 | 141.606 | 99.288 |
| $N$ | | 7 | 5 | 5 |
| Fraction | $S$ | 0.551 | 0.568 | 0.601 |
| | $E$ | 0.449 | 0.432 | 0.399 |
| $r^2_{\mathrm{bs}}$ | | 0.969 | 0.959 | 0.947 |
| $\mathrm{SD}_{\mathrm{bs}}$ | | 0.013 | 0.015 | 0.014 |
| $r^2_{\mathrm{CV(mean)}}$ | | 0.675 | 0.545 | 0.522 |

$q^2$ = cross-validated correlation coefficient; $s_{\mathrm{press}}$ = cross-validated standard error; $r^2$ = determination coefficient; SEE = noncross-validated standard error; $F$ = Fischer's $F$-value; $N$ = optimal number of components; Fraction = relative contribution of the fields, $r^2_{\mathrm{bs}} = r^2$ obtained after bootstrapping; $\mathrm{SD}_{\mathrm{bs}}$ = bootstrapping standard deviation; $r^2_{\mathrm{CV(mean)}}$ = mean $r^2$ of cross-validation in groups.

**Table 4**
PLS statistics of different CoMSIA models generated using alignment 1

| Parameters | | SE[a] | SH[b] | EH[c] | SEH[d] | H |
|---|---|---|---|---|---|---|
| $q^2$ | | 0.732 | 0.565 | 0.566 | 0.641 | 0.543 |
| $s_{press}$ | | 0.546 | 0.680 | 0.671 | 0.624 | 0.688 |
| $r^2$ | | 0.939 | 0.920 | 0.865 | 0.936 | 0.882 |
| SEE | | 0.261 | 0.292 | 0.374 | 0.265 | 0.350 |
| $F$ | | 71.620 | 84.042 | 48.227 | 77.965 | 55.963 |
| $N$ | | 9 | 7 | 6 | 8 | 6 |
| Fraction | $S$ | 0.449 | 0.428 | – | 0.262 | – |
| | $E$ | 0.551 | – | 0.471 | 0.391 | – |
| | $H$ | – | 0.572 | 0.529 | 0.347 | 1.000 |
| $r^2_{bs}$ | | 0.969 | 0.969 | 0.900 | 0.957 | 0.918 |
| $SD_{bs}$ | | 0.004 | 0.007 | 0.031 | 0.023 | 0.016 |
| $r^2_{CV(mean)}$ | | 0.714 | 0.538 | 0.526 | 0.627 | 0.529 |

$q^2$ = cross-validated correlation coefficient; $s_{press}$ = cross-validated standard error; $r^2$ = determination coefficient; SEE = noncross-validated standard error; $F$ = Fischer's $F$-value; $N$ = optimal number of components; Fraction = relative contribution of the fields, $r^2_{bs} = r^2$ obtained after bootstrapping; $SD_{bs}$ = bootstrapping standard deviation; $r^2_{CV(mean)}$ = mean $r^2$ of cross-validation in groups; [a]steric and electrostatic; [b]steric and hydrophobic; [c]electrostatic and hydrophobic; [d]steric and electrostatic and hydrophobic fields; $H$ = hydrophobic field.

### 3.1. CoMFA analysis

In 3D-QSAR CoMFA and CoMSIA studies a $q^2$ of 0.3 is considered statistically significant [20] however a $q^2$ value of 0.4 is generally considered better. In view of it, the CoMFA models having $q^2 > 0.5$ can be considered significant statistically. The Tripos standard (TS) field showed the highest $q^2$ of 0.733 using 7 principal components with a high conventional $r^2$ value of 0.967 and low standard error of estimate (0.187) indicates a statistically highly significant model. To further assess the robustness of the models, bootstrapping analysis (100 runs) was performed and $r^2_{bs}$ of 0.969 ($SD_{bs}$ = 0.013) was obtained, further establishing the strength of the model.

In addition to LOO, a group cross-validation was further done to assess the internal predictive ability of the model, cross-validation for 10 times was performed with 10 groups and the mean $r^2_{CV}$ [$R^2_{CV(mean)}$] of 0.675 (TS) reveals that the models have good internal predictivity and the results were not based on chance correlation (Table 3).

### 3.2. Advanced CoMFA

In advanced CoMFA study, hydrogen bonding, indicator and parabolic fields were calculated. The HB did not give significant $q^2$ value and hence was dropped from further analysis. The indicator field showed a cross-validated $q^2$ of 0.604 with five components, $r^2$ of 0.939 with standard error of 0.249 and $F$-value of 141.606. The parabolic field gave a cross-validated $q^2$ of 0.556 with five components, $r^2$ of 0.915 with standard error of 0.293 and $F$-value of 99.288. As observed above these results are also highly significant.

To further assess the statistical robustness of the models, bootstrapping analysis (100 runs) was performed using the optimum number of components ($n$ = 5) and $r^2_{bs}$ of 0.959 (SD = 0.015) and 0.947(SD = 0.014) were obtained for indicator and parabolic fields, respectively. Cross-validation in groups was performed using 10 groups repeating the analysis 10 times and the mean $r^2_{CV}$ [$r^2_{CV(mean)}$] of 0.545 and 0.522 was obtained for the indicator and parabolic field descriptors, respectively. This further established good internal predictivity of the generated models (Table 3).

### 3.3. CoMSIA analysis

Various CoMSIA models were generated considering all possible combinations of field descriptors. In this study, steric ($S$), electrostatic ($E$) and hydrophobic ($H$) field descriptors were found to have important role in modulation of biological activity. Several of the models were found to have high statistical significance. The model having steric and electrostatic fields gave the highest $q^2$ of 0.732 at 9 components among generated CoMSIA models, while model developed using $S$, $E$ and $H$ gave a significant $q^2$ value of 0.641 with eight components and a conventional noncross-validated $r^2$ of 0.936 (Table 4).

To further assess the statistical ability and the robustness of the model, bootstrapping analysis (100 runs) was performed and $r^2_{bs}$ of 0.957 with low standard deviation of 0.023 was obtained showing robustness of the models. Similar to CoMFA, to assess the internal predictive ability of the model, group cross-validation was performed with 10 groups and the mean $r^2_{cv}$ [$r^2_{CV(mean)}$] of 0.627 reveals that these models have high internal predictivity.

### 3.4. External validation

The external validation is the most rigorous validation which consists of making for predictions of compounds not included in the training set; therefore this validation measures the true external predictivity of the generated models. As already mentioned the external validation in 3D-QSAR is utmost important [18a,b] and hence the test set of 26 compounds (Table 1) was used to assess the external predictivity of model.

The external predictive ability of the generated CoMFA model was evaluated in terms of predictive $r^2$ value ($r^2_{pred}$) as implied in Sybyl6.9. The Tripos standard field showed a high ($r^2_{pred}$) value of 0.732, while indicator and parabolic fields showed ($r^2_{pred}$) value of 0.773 and 0.622, respectively indicating the developed CoMFA models have very good external predictivity in addition to good internal predictivity. The observed and predicted activities of the training set and test set compounds by CoMFA (TS) model are shown in Table 5. Fig. 3 shows the graph of observed versus predicted activities of training set and test set by CoMFA (TS) model.

The CoMSIA models were also subjected to external validation similar to CoMFA. The CoMSIA model developed using combination of steric and electrostatic field showed good external predictive ability ($r^2_{pred} = 0.743$). The model consisting of steric, electrostatic and hydrophobic field showed the excellent external predictivity ($r^2_{pred}$ value) of 0.812 indicating a robust model. The other field combinations also showed good external predictivity ($r^2_{pred} > 0.70$). The observed and predicted activities of the training set and test set by the best CoMSIA (SEH) model are shown in Table 5. Fig. 4 shows the graph of observed and predicted activities

**Table 5**
Observed (Obs.), predicted AChE inhibitory activities ($pIC_{50}$) and residuals ($\delta$) of the best CoMFA (TS), advanced CoMFA (INN) and CoMSIA (SEH) models

| Comp. | Obs. | TS[±] | $\delta$ | IND[≠] | $\delta$ | SEH[†] | $\delta$ |
|---|---|---|---|---|---|---|---|
| 1 | 1.52 | 1.30 | 0.22 | 1.24 | 0.29 | 0.86 | 0.66 |
| 2* | 0.04 | −0.35 | 0.39 | −0.48 | 0.52 | −0.36 | 0.40 |
| 3* | 0.12 | 0.37 | −0.25 | 0.28 | −0.16 | 0.23 | −0.11 |
| 4 | −1.28 | −1.15 | −0.13 | −1.18 | −0.10 | −1.17 | −0.11 |
| 5* | −0.86 | −0.96 | 0.10 | −1.00 | 0.14 | −1.10 | 0.24 |
| 6 | 0.28 | 0.25 | 0.03 | 0.27 | 0.01 | 0.04 | 0.24 |
| 7* | −0.60 | −0.74 | 0.14 | −0.48 | −0.12 | −1.45 | 0.85 |
| 8 | 0.52 | 0.52 | 0.01 | 0.64 | −0.12 | 0.51 | 0.02 |
| 9* | −1.25 | −0.35 | −0.90 | −0.66 | −0.59 | −0.17 | −1.08 |
| 10 | −0.17 | −0.09 | −0.08 | −0.50 | 0.33 | −0.09 | −0.08 |
| 11* | −0.03 | −0.23 | 0.20 | −0.10 | 0.07 | −0.02 | −0.01 |
| 12 | −1.59 | −1.82 | 0.23 | −1.57 | −0.02 | −1.44 | −0.15 |
| 13* | −1.39 | −0.50 | −0.89 | −0.71 | −0.68 | −0.37 | −1.02 |
| 14* | −0.56 | −1.71 | 1.15 | −1.36 | 0.80 | −1.40 | 0.84 |
| 15 | 0.34 | 0.24 | 0.10 | 0.64 | −0.30 | 0.36 | −0.02 |
| 16* | −1.02 | −0.94 | −0.08 | −1.03 | 0.01 | −0.87 | −0.16 |
| 17* | 0.29 | 0.56 | −0.27 | 0.64 | −0.35 | 0.01 | 0.28 |
| 18 | 2.05 | 2.24 | −0.19 | 2.29 | −0.24 | 2.12 | −0.07 |
| 19* | 1.59 | 0.76 | 0.83 | 0.92 | 0.67 | 0.72 | 0.87 |
| 20 | −0.17 | −0.16 | −0.01 | −0.12 | −0.05 | −0.12 | −0.06 |
| 21* | −0.79 | −1.64 | 0.85 | −1.09 | 0.30 | −0.90 | 0.11 |
| 22 | −0.51 | −0.53 | 0.02 | −0.41 | −0.11 | −0.42 | −0.09 |
| 23* | −1.90 | −1.77 | −0.13 | −1.87 | −0.03 | −1.73 | −0.17 |
| 24 | −0.46 | −0.33 | −0.13 | −0.40 | −0.06 | −0.54 | 0.08 |
| 25* | −1.62 | −1.68 | 0.06 | −1.78 | 0.16 | −1.55 | −0.07 |
| 26 | −1.16 | −1.40 | 0.24 | −1.60 | 0.44 | −1.43 | 0.27 |
| 27 | −1.20 | −1.31 | 0.11 | −1.16 | −0.05 | −1.15 | −0.05 |
| 28 | −1.61 | −1.38 | −0.23 | −1.26 | −0.35 | −1.43 | −0.18 |
| 29* | 0.07 | −0.29 | 0.36 | −0.51 | 0.58 | 0.09 | −0.02 |
| 30 | −1.14 | −1.20 | 0.06 | −1.46 | 0.32 | −0.96 | −0.18 |
| 31 | −0.38 | −0.34 | −0.04 | −0.63 | 0.25 | −0.43 | 0.05 |
| 32 | −1.05 | −0.96 | −0.10 | −1.15 | 0.10 | −1.02 | −0.03 |
| 33* | −1.86 | −0.98 | −0.88 | −0.72 | −1.14 | −1.89 | 0.03 |
| 34 | −1.25 | −1.15 | −0.11 | −1.33 | 0.08 | −1.19 | −0.06 |
| 35 | −0.25 | −0.39 | 0.14 | −0.21 | −0.04 | −0.14 | −0.11 |
| 36* | 0.26 | −0.82 | 1.08 | 0.04 | 0.22 | −0.06 | 0.32 |
| 37 | −1.11 | −0.77 | −0.34 | −0.61 | −0.50 | −0.48 | −0.63 |
| 38 | −1.25 | −1.31 | 0.06 | −1.12 | −0.13 | −1.37 | 0.12 |
| 39 | −0.40 | −0.86 | 0.46 | −0.94 | 0.54 | −0.83 | 0.43 |
| 40 | −2.72 | −2.06 | −0.66 | −2.33 | −0.39 | −2.14 | −0.58 |
| 41 | −1.66 | −1.64 | −0.02 | −1.88 | 0.22 | −2.02 | 0.36 |
| 42 | −0.85 | −0.71 | −0.14 | −0.86 | 0.01 | −0.72 | −0.13 |
| 43* | −2.64 | −1.92 | −0.72 | −2.20 | −0.44 | −2.21 | −0.43 |
| 44* | 1.28 | 1.17 | 0.11 | 1.57 | −0.29 | 1.03 | 0.26 |
| 45 | −0.33 | −0.28 | −0.05 | −0.10 | −0.23 | −0.22 | −0.12 |
| 46 | −1.41 | −1.60 | 0.19 | −1.36 | −0.06 | −1.38 | −0.03 |
| 47 | −1.64 | −1.60 | −0.04 | −1.65 | 0.01 | −1.41 | −0.23 |
| 48 | −0.25 | −0.31 | 0.06 | −0.62 | 0.37 | −0.54 | 0.29 |
| 49 | −0.60 | −0.61 | 0.01 | −1.12 | 0.52 | −1.00 | 0.40 |
| 50* | −1.72 | −1.88 | 0.16 | −1.93 | 0.21 | −2.28 | 0.56 |
| 51 | −0.61 | −0.60 | −0.01 | −0.89 | 0.28 | −0.87 | 0.26 |
| 52 | −2.31 | −2.30 | −0.01 | −2.18 | −0.13 | −2.28 | −0.03 |
| 53 | −1.17 | −1.26 | 0.09 | −0.95 | −0.22 | −1.29 | 0.12 |
| 54 | −0.33 | −0.25 | −0.08 | −0.47 | 0.14 | 0.03 | −0.36 |
| 55* | 1.89 | 1.55 | 0.34 | 0.98 | 0.91 | 1.53 | 0.36 |
| 56 | 0.64 | 0.62 | 0.02 | 0.59 | 0.05 | 0.45 | 0.19 |
| 57 | −1.55 | −1.51 | −0.04 | −1.13 | −0.42 | −1.55 | 0.00 |
| 58 | −0.89 | −0.94 | 0.05 | −0.90 | 0.01 | −1.19 | 0.30 |
| 59 | 0.55 | 0.67 | −0.12 | 0.37 | 0.18 | 0.79 | −0.24 |
| 60* | −1.32 | −1.73 | 0.41 | −0.90 | −0.42 | −1.62 | 0.30 |
| 61 | 0.76 | 0.75 | 0.02 | 0.68 | 0.08 | 0.60 | 0.16 |
| 62 | 0.66 | 0.48 | 0.18 | 0.44 | 0.22 | 0.78 | −0.12 |
| 63 | −1.48 | −1.52 | 0.04 | −1.19 | −0.29 | −1.12 | −0.36 |
| 64 | −1.19 | −0.97 | −0.22 | −1.00 | −0.19 | −1.07 | −0.12 |
| 65* | 0.07 | 0.25 | −0.18 | 0.23 | −0.16 | 0.18 | −0.11 |
| 66 | −1.22 | −1.45 | 0.23 | −1.43 | 0.21 | −1.38 | 0.16 |
| 67 | 0.27 | 0.02 | 0.26 | −0.08 | 0.35 | 0.19 | 0.09 |
| 68 | −1.53 | −1.46 | −0.08 | −1.53 | 0.00 | −1.43 | −0.10 |
| 69 | −1.28 | −1.44 | 0.16 | −1.63 | 0.35 | −1.50 | 0.22 |
| 70* | −0.56 | −1.01 | 0.45 | −1.22 | 0.66 | −0.82 | 0.26 |
| 71 | −1.09 | −0.97 | −0.12 | −0.95 | −0.14 | −1.23 | 0.14 |
| 72* | −0.22 | −0.42 | 0.20 | −0.36 | 0.14 | −0.25 | 0.03 |
| 73 | −2.37 | −2.53 | 0.16 | −2.12 | −0.25 | −2.35 | −0.03 |
| 74 | −1.52 | −1.40 | −0.12 | −1.52 | 0.00 | −1.26 | −0.26 |
| 75 | −0.49 | −0.56 | 0.07 | −0.26 | −0.23 | −0.51 | 0.02 |

**Table 5** (*Continued*)

| Comp. | Obs. | TS[±] | δ | IND[≠] | δ | SEH[†] | δ |
|---|---|---|---|---|---|---|---|
| 76 | −0.94 | −1.05 | 0.11 | −0.89 | −0.05 | −1.05 | 0.11 |
| 77* | 0.77 | 0.39 | 0.38 | −0.02 | 0.79 | 0.52 | 0.25 |
| 78 | −1.14 | −1.17 | 0.03 | −1.15 | 0.01 | −1.13 | −0.01 |
| $r^2_{pred}$ | | 0.73 | | 0.73 | | 0.81 | |

*Compounds of the test set; $r^2_{pred}$ = predictive $r^2$; [±]TS = Tripos standard field; [≠]IND = indicator field; [†]*S* = steric, *E* = electrostatic, *H* = hydrophobic field.

of training set and test set by CoMSIA (SEH) model. The impressive results obtained for these test-set compounds provide strong evidence that the CoMFA and CoMSIA models so derived are able to predict well the AChE inhibitory activities of structurally diverse carbamates taken in the study.

### 3.5. CoMFA and CoMSIA contour maps

The analysis of the CoMFA and CoMSIA contour maps provides good insight into the SAR by providing a visual display of favoured and disfavoured positions. Therefore, the steric and electrostatic features of the final CoMFA and CoMSIA models are displayed as contour maps of the PLS regression coefficients at each CoMFA/CoMSIA region grid point. They are generated using the field type *StDev*Coefficient* to show the contribution for favourable and unfavourable interactions with the receptor in terms of steric (80% green, 20% yellow), electrostatic (80% blue and 20% red) and hydrophobic (80% yellow, 20% white). These contour maps for the 3D models are shown in Figs. 5–10.

The surfaces near the template molecule (**18**) indicate the regions where the increase (green region) or decrease (yellow region) in steric bulk as well as increase (blue region) or decrease (red region) in electrostatic field would be important for the improvement of binding affinity. The yellow polyhydra in the hydrophobic contours shows the region where an increase in hydrophobicity is favourable for AChE inhibitory activity while white polyhydra denotes the region where hydrophobicity is unfavourable for activity. The advantage of CoMSIA contour maps over CoMFA is that they are easier to interpret.

The contours on the molecules are divided into two groups. The group one consists of contours which are enclosing or are near to the carbamate group (site 1), the second groups consists of the contours at or near the indane moiety (site 2) (Fig. 5A and B).

### 3.6. Contour maps on site 1

The blue polyhydra around carbamoyl nitrogen in contours of both CoMFA (Fig. 5A) as well as CoMSIA (Fig. 5B) indicate that this nitrogen should be more electropositive for better binding with AChE enzyme. Therefore, the electron withdrawing groups on this nitrogen should be more favourable for biological activity. It can easily be seen among nonpropargyl 6-carbamates, e.g. compound 8 ($IC_{50}$ = 0.30 μM), which has 4-methoxyphenyl (*p*-MeOPh) as $R_4$ ($IC_{50}$ = 0.76 μM), is about 2 times more potent than the compound 3 substituted with methyl (Me) as $R_4$. This may be due to the fact that *p*-MeOPh group pull away electrons from carbamoyl nitrogen through resonance and thereby rendering the nitrogen more electropositive; Among propargylated 6-carbamates also, this observation is consistent, e.g. compound 29 ($IC_{50}$ = 0.86 μM), which has *p*-MeOPh as $R_4$, is about 45 fold more potent than compound 28 ($IC_{50}$ = 41.2 μM) substituted with cyclohexyl group as $R_4$.

The bigger green polyhydra in both CoMFA as well as CoMSIA contours suggest that bulkier groups extending to this region (site 1) would be more favourable for better AChE inhibitory activity. It

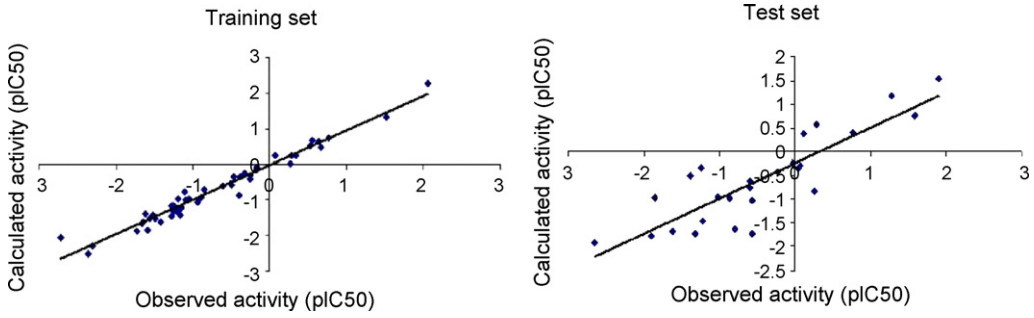


**Fig. 3.** The graph of observed versus calculated activities of training set and test set compounds using the best CoMFA (TS) model.

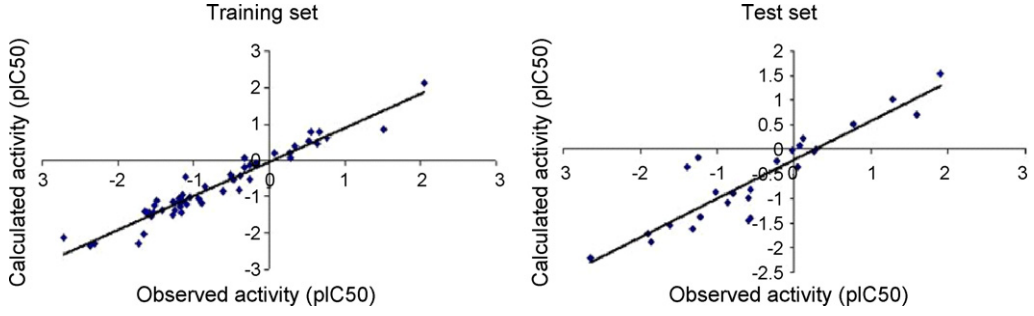


**Fig. 4.** The graph of observed versus calculated activities of training set and test set compounds using the best CoMSIA (SEH) model.

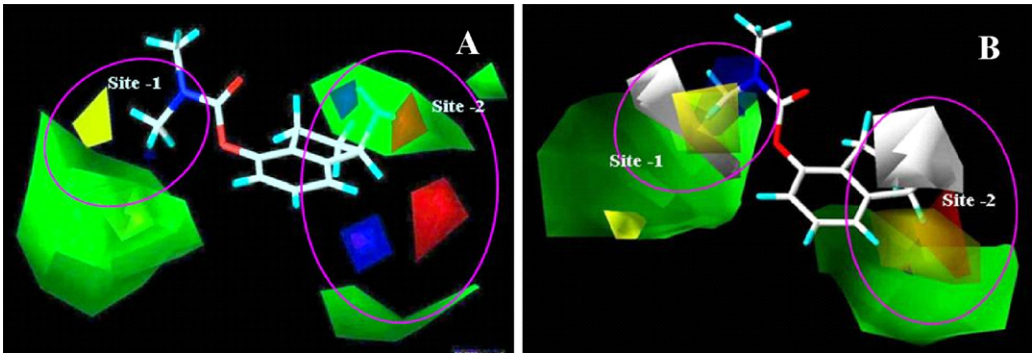


**Fig. 5.** (A) Contour map of the best CoMFA model using Tripos standard field and (B) contour map of the best CoMSIA model using steric, electrostatic and hydrophobic fields.

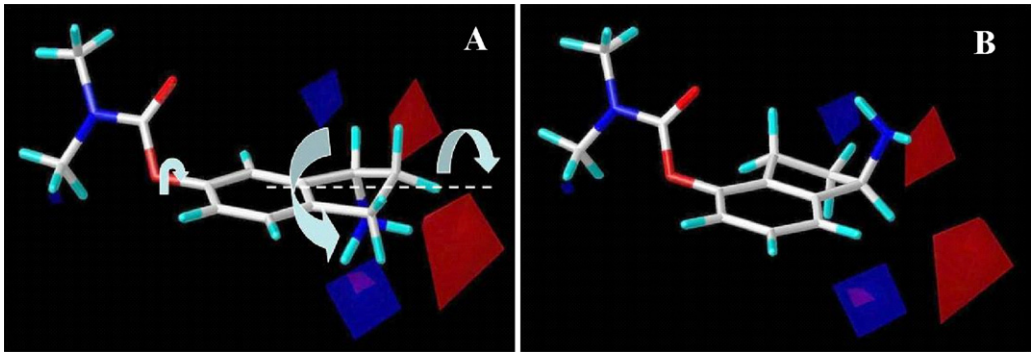


**Fig. 6.** (A) Electrostatic contour maps of the best CoMFA (TS) model displayed around compound 3 and (B) electrostatic contour maps of the best CoMFA (TS) model displayed around compound 18.

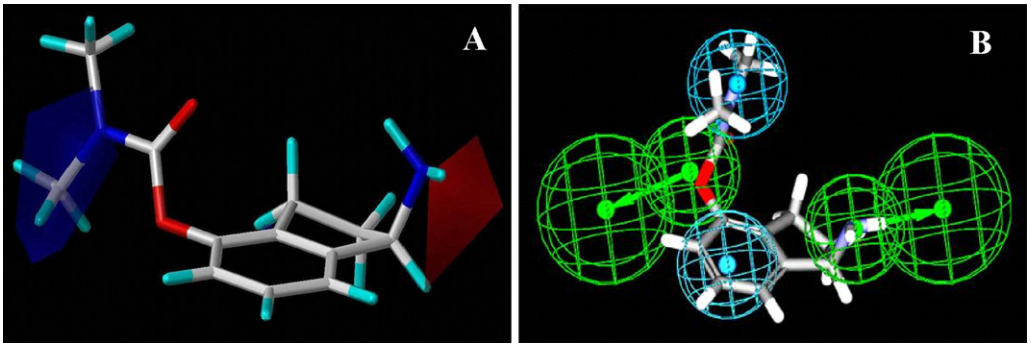


**Fig. 7.** (A) Electrostatic contour map of the best CoMSIA model displayed around compound 18 and (B) the common feature pharmacophore model generated using Catalyst software (blue sphere indicate hydrophobic feature, while green sphere are indicative of hydrogen bond acceptor (HBA) feature with the arrow showing the directionality of the acceptor feature).

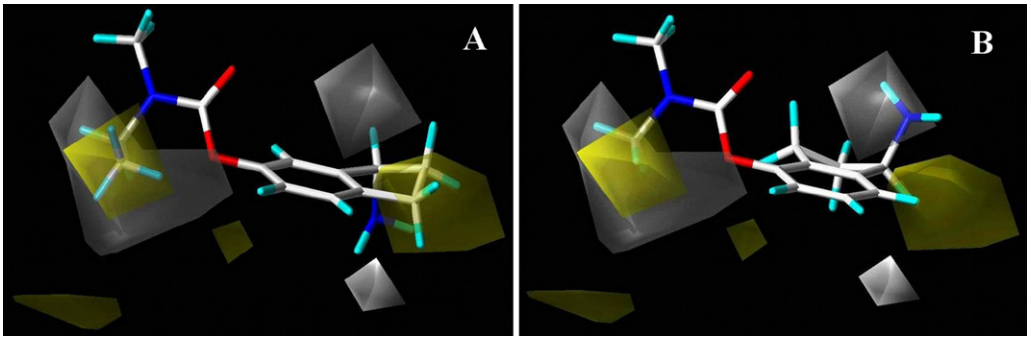


**Fig. 8.** (A) Hydrophobic contour maps of the best CoMSIA (SEH) model displayed around compound 3 and (B) hydrophobic contour maps of the best CoMSIA (SEH) model displayed around compound 18.

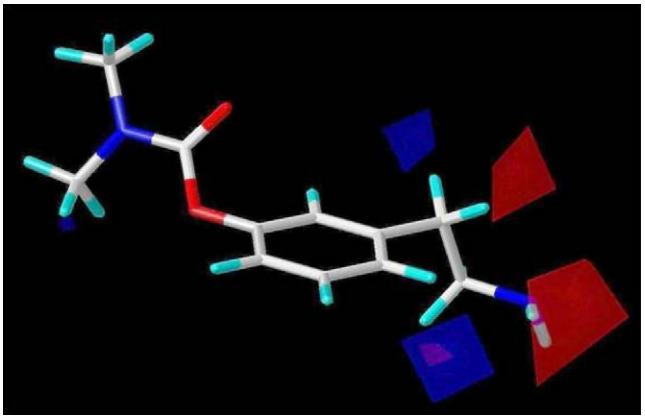

**Fig. 9.** Electrostatic contour map of CoMFA displayed around compound 56.

is particularly interesting to note that a yellow polyhydra enclosed by a bigger green polyhydra near carbamoyl nitrogen appears both in CoMFA and CoMSIA contour maps. It explains the anomalous effect of ethyl group on AChE inhibitory activity *i.e.* ethyl group is disfavourable for binding with AChE while methyl or propyl groups are favourable. This has previously been reported by Weinstock et al. [12,13]. for a series of mono- and dialkyl-3-(1-dimethylaminoethyl)-phenylcarbamates and by Leiske et al. [14]. for a series of 5-(1,3,3-trimethylindolinyl) carbamates. This anomalous ethyl effect is responsible for the observed contours and is prominent in SAR data, e.g. compound 3 ($R_4$ = Me; $IC_{50}$ = 0.76 μM) compound 5 ($R_4$ = Propyl; $IC_{50}$ = 7.38 μM) and compound 6 ($R_4$ = *n*-hexyl; $IC_{50}$ = 0.53 μM) are approx. 25, 3 and 36 times more active than compound 4 ($R_4$ = Et; $IC_{50}$ = 19 μM), respectively.

The yellow contour near carbamoyl nitrogen in CoMSIA contour map indicates that the hydrophobic groups (e.g. aromatic rings like phenyl, *p*-MeOPh, benzyl, etc.) which can extend to this region should be favourable for biological activity, e.g. compound 29 ($R_4$ = *p*-MeOPh; $IC_{50}$ = 0.86 μM) is about 50 times more potent than compound 28 ($R_4$ = cyclohexyl; $IC_{50}$ = 41.2 μM).

Considering all the above observations for *site 1* together it can be inferred that an ideal group here should have good electron withdrawing power to make the carbamoyl nitrogen more electropositive and it should have higher steric bulk and hydrophobicity. The groups like *p*-MeOPh or other bulky electron withdrawing groups along with high hydrophobicity may lead to improved AChE inhibitory activity.

### 3.7. Contour maps on site 2

The blue and red polyhydra above and below the dashed line (Fig. 6A and B) are arising due to the opposite orientation of the amino nitrogen of 4- and 6-carbamates in 3D space in the chosen alignment scheme where all molecules in the dataset are aligned keeping the carbamate groups in one place. Thus, due to the opposite orientation of amino nitrogen in the two groups of molecules, two blue and two red polyhydra are seen. A close examination of these contours reveals that they may be the part of one blue and one red polyhydra had the C–O bond is rotated in some compounds to bring all nitrogen on one side (Fig. 6A). However in the CoMSIA electrostatic contour (Fig. 7A) only a red polyhydra is seen near the amino nitrogen. In order to resolve this ambiguity further a pharmacophore model was developed for these molecules using a representative set consisting of 28 molecules (covering different features in the dataset, Table 6) by Catalyst (HipHop) where the blue sphere indicate hydrophobic feature, while green ones are indicative of hydrogen bond acceptor (HBA) feature with the arrow showing the directionality of the acceptor feature. The observed green sphere around amino nitrogen clearly shows a hydrogen bond acceptor in this region (Fig. 7B) and explains the high activity of the molecules having dimethyl substitution at this nitrogen. This pharmacophore shows a hydrophobic feature on dimethyl amino group of the carbamate which corresponds well with the CoMFA (steric) and CoMSIA

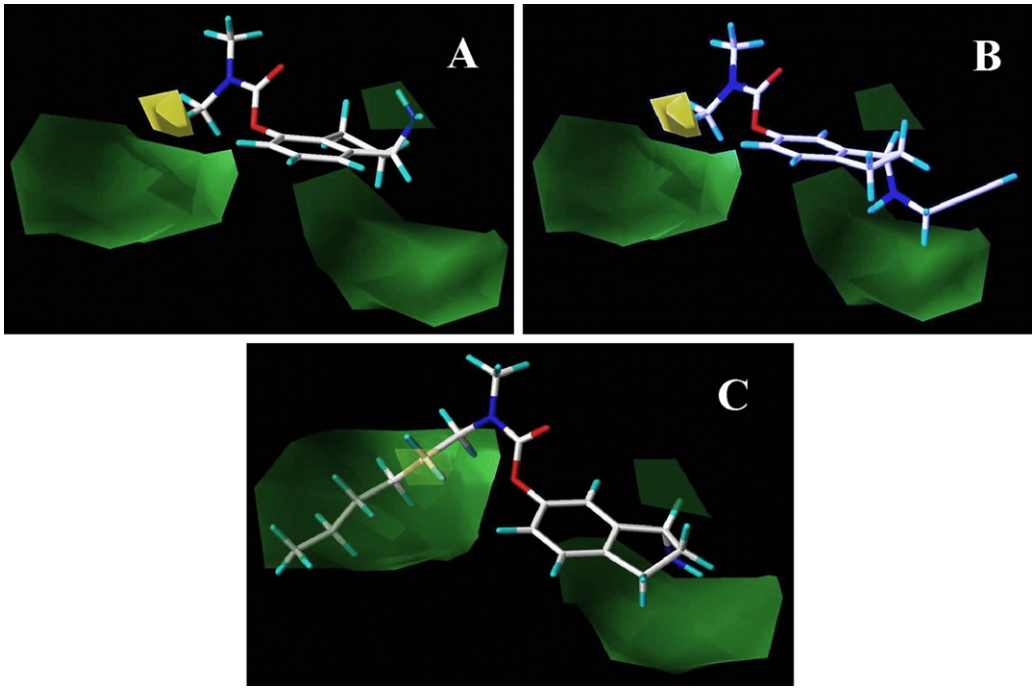


**Fig. 10.** (A) Steric contour maps of the best CoMSIA (SEH) model displayed around compound 18; (B) steric contour maps of the best CoMSIA (SEH) model displayed around compound 6 and (C) steric contour maps of the best CoMSIA (SEH) model displayed around compound 24.

**Table 6**
The compounds taken for Catalyst pharmacophore generation

| S. No. | Comp. | $IC_{50}$ | S. No. | Comp. | $IC_{50}$ |
|---|---|---|---|---|---|
| 1 | 1 | 0.03 | 15 | 53 | 14.90 |
| 2 | 8 | 0.30 | 16 | 55 | 0.013 |
| 3 | 18 | 0.009 | 17 | 56 | 0.23 |
| 4 | 19 | 0.026 | 18 | 59 | 0.28 |
| 5 | 21 | 6.22 | 19 | 61 | 0.16 |
| 6 | 22 | 3.24 | 20 | 65 | 0.85 |
| 7 | 24 | 2.90 | 21 | 67 | 0.54 |
| 8 | 27 | 15.70 | 22 | 69 | 19.10 |
| 9 | 29 | 0.86 | 23 | 70 | 3.60 |
| 10 | 34 | 17.90 | 24 | 72 | 1.64 |
| 11 | 40 | 525.00 | 25 | 73 | 234.00 |
| 12 | 46 | 25.50 | 26 | 74 | 33.10 |
| 13 | 49 | 3.94 | 27 | 75 | 2.00 |
| 14 | 51 | 4.10 | 28 | 77 | 0.17 |

(hydrophobic) contours at site 1. However the pharmacophore model has another HBA feature on oxygen of carbamate group for which no corresponding contour on CoMFA and CoMSIA models was seen. The hydrophobic feature which is coming on the aromatic ring of pharmacophore model also does not have any corresponding CoMFA and CoMSIA contour. Since all the molecules in the dataset have been aligned over the same core, these features are common, therefore no distinguishing CoMFA and CoMSIA contours can be observed.

It may be inferred from the above observations that the amino nitrogen at site 2 should be more electronegative so that it can act as HB acceptor and the substitutions should be made accordingly at this position for better AChE inhibitory activity. On the other hand a red polyhydra is seen around the nitrogen of the molecules having amino group attached to phenethyl moiety (Fig. 9). This indicates that negative nitrogen is therefore required for better inhibitory activity. The amino nitrogen when disubstituted with methyl group will act as hydrogen bond acceptor rather than donor. It also suggests that there may be improvement in AChE binding when the amino nitrogen is disubstituted.

The yellow contour around closed ring of 6-carbamates in site 2 (Fig. 8A and B) indicates that hydrophobicity in this region has favourable effect on the AChE inhibitory activity. Thus molecules having a hydrophobic group (e.g. indane and tetralene derivatives) here may be more favourable towards AChE inhibition.

The white polyhydra around the amino nitrogen of 4- and 6-carbamates (Fig. 8A and B) gave an insight about the possibility of enhancement of AChE inhibitory activity by putting more hydrophilic groups. This contour also gave an explanation of why molecules with free amino group *i.e.* primary amino group also led to enhanced activity.

The wide green contour (Fig. 10A–C) below the plane somewhat near amino nitrogen in site 2 indicates that steric group in this site may be favourable among 6-carbamates. In Fig. 10A the most active compound is shown. It can be reasonably expected that the derivatives having some steric bulk which can reach to this region may show better activity. We are giving more emphasis on the 6-carbamates due to the fact that about 2/3rd of the data set is of 6-carbamates. Also it is evident from contours that a small green polyhydra is present near amino nitrogen of 4-carbamates indicate that steric group may have favourable impact on AChE inhibitory activity.

## 4. Conclusion

The CoMFA, advanced CoMFA and CoMSIA method has been applied successfully to rationalize the anti-AChE activity of structurally diverse carbamate based AChE inhibitors covering a wide range of biological activity and structural features in terms of their steric, electrostatic, hydrophobic, donor and acceptor properties. To the best of our knowledge no systematic QSAR study using CoMFA and CoMSIA has been reported on carbamates as AChE inhibitors, therefore this is the first attempt to explore the structure activity relationship of carbamate based AChE inhibitors using these techniques. The developed models showed good statistical significance in internal ($q^2$, group cross-validation and bootstrapping) validation and performed very well in predicting the biological activity ($pIC_{50}$) of the compounds in the test set. After the detailed study of the CoMFA, advanced CoMFA and CoMSIA contours, it can be concluded that electron withdrawing groups having some steric bulk (phenyl, substituted phenyl, etc.) may lead to compounds with higher activity among 4-carbamates and this can be suggested as a novel finding of this study. It is hoped that these models can help in future design and optimization of AChE inhibitors for the treatment of the AD.

## Acknowledgements

The author (KKR) is thankful to the Indian Council of Medical Research (ICMR) Delhi, India for the financial assistance in the form of fellowship to pursue research on the Alzheimer's disease. The technical assistance of Mr. A.S. Kushwaha is also acknowledged.

## Appendix A. Supplementary data

Supplementary data associated with this article can be found, in the online version, at doi:10.1016/j.jmgm.2008.04.006.

## References

[1] J.T. Coyle, D.L. Price, M.R. DeLong, Alzheimer's disease: a disorder of cortical cholinergic innervation, Science 219 (1983) 1184–1190.
[2] D.M. Quinn, S.R. Feaster, H.K. Nair, N.A. Baker, Z. Radic, P. Taylor, Delineation and decomposition of energies involved in quaternary ammonium binding in the active site of acetylcholinesterase, J. Am. Chem. Soc. 122 (2000) 2975–2980.
[3] M. Ballmaier, F. Casamenti, C. Scali, R. Mazzoncini, M. Zoli, Rivastigmine antagonizes deficits in prepulse inhibition induced by selective immunolesioning of cholinergic neurons in nucleus basalis magnocellularis, Neuroscience 114 (2002) 91–98.
[4] C.A. Barnes, J. Meltzer, F. Houston, G. Orr, K. McGann, Chronic Treatment of old rats with donepezil or galantamine: effects on memory. hippocampal plasticity and nicotinic receptors, Neuroscience 99 (2000) 17–23.
[5] D. Van Dam, D. Abramowski, M. Staufenbiel, P.P. De Deyn, Symptomatic effect of donepezil, rivastigmine. Galantamine and memantine on cognitive deficits in the APP23 Model, Psychopharmacology (Berl.) 180 (2005) 177–190.
[6] A. Clegg, J. Bryant, T. Nicholson, L. McIntyre, S. De Broe, K. Gerard, N. Waugh, Clinical and cost-effectiveness of donepezil. Rivastigmine and Galantamine for Alzheimer's disease: a rapid and systematic review, Health Technol. Assess. 5 (2001) 1–137.
[7] A. Clegg, J. Bryant, T. Nicholson, L. McIntyre, S. De Broe, K. Gerard, N. Waugh, Clinical and cost-effectiveness of donepezil. Rivastigmine and galantamine for Alzheimer's disease, Int. J. Technol. Assess. Health Care 18 (2002) 497–507.
[8] B. Goldlist, M. Gordon, G. Naglie, Galantamine vs donepezil in the treatment of Alzheimer's disease, Drugs Aging 20 (2003) 1139–1140.
[9] V.P. Prasher, Review of donepezil: ageing and health issues in intellectual disabilities, Int. J. Geriatr. Psychiatry 19 (2004) 509–515.
[10] J.L. Sussman, M. Harel, F. Frolow, C. Oefner, A. Goldman, L. Toker, I. Silman, Atomic structure of acetylcholinesterase from torpedo californica: a prototypic acetylcholine-binding protein, Science 253 (1991) 872–879.
[11] D.M. Quinn, Acetylcholinesterase–enzyme structure, reaction dynamics, and virtual transition-states, Chem. Rev. 87 (1987) 955–979.
[12] M. Weinstock, M. Razin, I. Ringel, Z. Tashma, M. Chorev, Acetylcholinesterase inhibition by novel carbamates: a kinetic and nmr study, in: A. Shafferman, B. Velan (Eds.), Multidiscipinary Approaches to Cholinesterase Functions, 36th edn., Plenum, New York, NY, 1992, pp. 251–259.
[13] M. Weinstock, M. Razin, M. Chorev, Z. Tashma, Pharmacological activity of novel anticholinesterase agents of potential use in treatment of Alzheimer's disease, J. Neural. Transm. 43 (1994) 219–225.

[14] C.N. Lieske, R.T. Gepp, J.H. Clark, H.G. Meyer, P. Blumberg, C.C. Tseng, Anticholinesterase activity of potential therapeutic 5-(1,3,3-Trimethylindolinyl) carbamates, J. Enzyme Inhib. 5 (1991) 215–223.
[15] G. Lin, G.H. Chen, S.C. Yeh, C.P. Lu, Probing the peripheral anionic site of acetylcholinesterase with quantitative structure activity relationships for inhibition by biphenyl-4-acyoxylate-4-*N*-butylcarbamates, J. Biochem. Mol. Toxicol. 19 (2005) 234–243.
[16] G. Lin, G.H. Chen, C.P. Lu, S.C. Yeh, QSARs for Peripheral anionic site of butyrylcholinesterase with inhibitions by 4-acyloxy-biphenyl-4′-*N*-butylcarbamates, QSAR Comb. Sci. 24 (2005) 943–952.
[17] J. Sterling, Y. Herzig, T. Goren, N. Finkelstein, D. Lerner, W. Goldenberg, I. Miskolczi, S. Molnar, F. Rantal, T. Tamas, G. Toth, A. Zagyva, A. Zekany, G. Lavian, A. Gross, R. Friedman, M. Razin, W. Huang, B. Krais, M. Chorev, M.B. Youdim, M. Weinstock, Novel dual inhibitors of ache and mao derived from hydroxy aminoindan and phenethylamine as potential treatment for Alzheimer's disease, J. Med. Chem. 45 (2002) 5260–5279.
[18] (a) A. Golbraikh, A. Tropsha, Beware of $q^2$! J. Mol. Graph. Model. 20 (2002) 269–276;
(b) P. Prathipati, K. Saxena Anil, Comparison of MLR. PLS and GA-MLR in QSAR analysis, SAR QSAR Environ. Res. 14 (2003) 433–446.
[19] Tripos Inc., South Hanley Road, St. Louis, MO 63144, 1699.
[20] M. Bohm, J. Sturzebecher, G. Klebe, Three-dimensional quantitative structure–activity relationship analysis using comparative molecular field analysis and comparative molecular similarity indices analysis to elucidate selectivity differences of inhibitors binding to trypsin, thrombin, and factor Xa, J. Med. Chem. 42 (1999) 458–477.
[21] R.D. Crammer, D.E. Patterson, J.D. Bunce, Comparative Molecular Field Analysis (CoMFA). 1. Effect of shape on binding of steroids to carrier proteins, J. Am. Chem. Soc. 110 (1988) 5959–5967.
[22] R.S. Bohacek, C. McMartin, Definition and display of steric, hydrophobic, and hydrogen-bonding properties of ligand binding sites in proteins using lee and richards accessible surfaces: validation of a high-resolution tool for drug design, J. Med. Chem. 35 (1992) 1671–1684.
[23] R.T. Kroemer, P. Hecht, Replacement of steric potential-derived interaction energies by atom-based indicator variables in CoMFA leads to models of higher consistency, J. Comput. Aided Mol. Des. 9 (1995) 205–221.
[24] G. Klebe, U. Abraham, T. Mietzner, Molecular similarity indices in a comparative analysis (CoMSIA) of drug molecules to correlate and predict their biological activity, J. Med. Chem. 37 (1994) 4130–4146.
[25] C.L. Waller, T.I. Oprea, A. Giolitti, G.R. Marshall, Three-dimensional QSAR of human immunodeficiency virus (I) Protease inhibitors. 1. A CoMFA study employing experimentally determined alignment rules, J. Med. Chem. 36 (1993) 4152–4160.
[26] R.D. Cramer, J.D. Bunce, D.E. Patterson, Cross-validation, bootstrapping, and partial least squares compared with multiple regression in conventional QSAR studies, Quant. Struct. Act. Relat. 7 (1988) 18–25.